Electronic Supplementary Material (ESI) for Lab on a Chip.

Electronic Supplementary Information

Modular soft robotic microdevices for dexterous biomanipulation

Berna Özkale[a,b,c], Raquel Parreira[a], Ahmet Bekdemir[d], Lucio Pancaldi[a], Ece Özelçi[a], Claire Amadio[a], Murat Kaynak[a], Francesco Stellacci[d,e], David J. Mooney[b,c] and Mahmut Selman Sakar[a,e,*]

[a] Institute of Mechanical Engineering, Ecole Polytechnique Fédérale de Lausanne (EPFL), CH-1015 Lausanne, Switzerland. Email: selman.sakar@epfl.ch

[b] Wyss Institute for Biologically Inspired Engineering, Harvard University, Cambridge, Massachusetts 02138, USA.

[c] School of Engineering and Applied Sciences, Harvard University, Cambridge, Massachusetts 02138, USA.

[d] Institute of Materials, EPFL, CH-1015 Lausanne, Switzerland.

[e] Institute of Bioengineering, EPFL, CH-1015 Lausanne, Switzerland.

Materials. Gold(III) chloride trihydrate (HAuCl4, 99.99%), hexadecyltrimethylammonium bromide (CTAB, 98%), sodium borohydride (99.99%), sodium oleate (95%), silver nitrate (99.0%), hydrochloric acid (HCl, 37%), L-ascorbic acid, N-isopropylmethacrylamide (NIPMAM), N,N'-methylenebisacrylamide, 2,2' azobis(2-methylpropionamidine) dihydrochloride (AAPH), allylamine, glutaraldehyde solution (50% in water), 1H,1H,2H,2H-perfluoro-1-octanol (PFO), poly(ethylene glycol) diacrylate (PEGDA, 700 kDa), 2-Hydroxy-2-methylpropiophenone (DAROCUR), and polydimethylsiloxane (PDMS) SYLGARD 184 kit were all purchased from Sigma Aldrich. N,N' -bis(acryloyl)cystamine was acquired from Alfa Aesar. Novec 7500 engineered fluid, the fluorinated oil, was purchased from 3M. The surfactant Pico-Surf was acquired from Dolomite Microfluidics. All chemicals were used as received.

Synthesis and characterization of the nanoactuators. The nanoactuators were synthesized according to a reported procedure[1]. We first synthesized gold nanorods (Au NRs) using CTAB capped seed nanoparticles in the presence of silver nitrate ($AgNO_3$) and sodium oelate (NaOL) as the secondary surfactant. Gold nanorods were coated with pNIPMAM by in situ free radical polymerization. The reaction was scaled up by a factor of 12 compared to the previously published report[1] and minor changes were implemented. Briefly, 180 ml milli-Q-water was heated up to 70 °C under constant stirring (700 rpm) and purged with N_2 for 30 minutes. A reflux column was inserted and 1.2g NIPMAM followed by 0.12g N,N'-methylenebisacrylamide were added while stirring. The stirring speed was increased to 1400 rpm and 12 ml of gold nanorod solution were directly injected into the solution. After 1 minute of stirring, 960 µl of 0.1 M AAPH were added and the reaction was allowed to proceed for 120 minutes under continuous N_2 purging with stirring at 1400 rpm. Following the first 30 minutes of the reaction, 120 µl allylamine diluted in 1 ml of milli-Q-water were added to the mixture. The solution was removed and allowed to cool down to room temperature while stirring. The

resulting nanoparticle solution was centrifuged at 5000 rpm for 30 minutes (10 °C), the supernatant was removed, and the pellet was re-dispersed in milli-Q-water. The washing steps were repeated three times and the solution was concentrated to 4 ml, this was the stock solution for microactuator fabrication.

The nanoactuators were characterized by transmission electron microscopy (TEM), ultraviolet-vis (UV-vis), and dynamic light scattering (DLS) measurements. TEM analysis was done using TALOS (FEI) at an operating voltage of 200 kV and 80 kV for gold nanorods and for the pNIPMAM coated gold nanorods, respectively. Negative staining with uranyl acetate was done on pNIPMAM coated gold nanorods prior to imaging. Both samples were basically prepared by drying a droplet onto a TEM copper grid. UV-vis measurements were carried out to measure the absorption of the nanoactuators using the V-670 UV-vis-NIR (Jasco) spectrophotometer over 20-70°C. DLS measurements were performed with Malvern Zetasizer Nano (Zen 3600) in milli-Q-water. Three measurements per temperature data point were taken on the same sample according to colloidal gold optical parameters.

References

[1] Z. Liu, Y. Liu, Y. Chang, H. R. Seyf, A. Henry, A. L.Mattheyses, K. Yehl, Y. Zhang, Z. Huang and K. Salaita, *Nature methods*, 2015, **13**, 143.

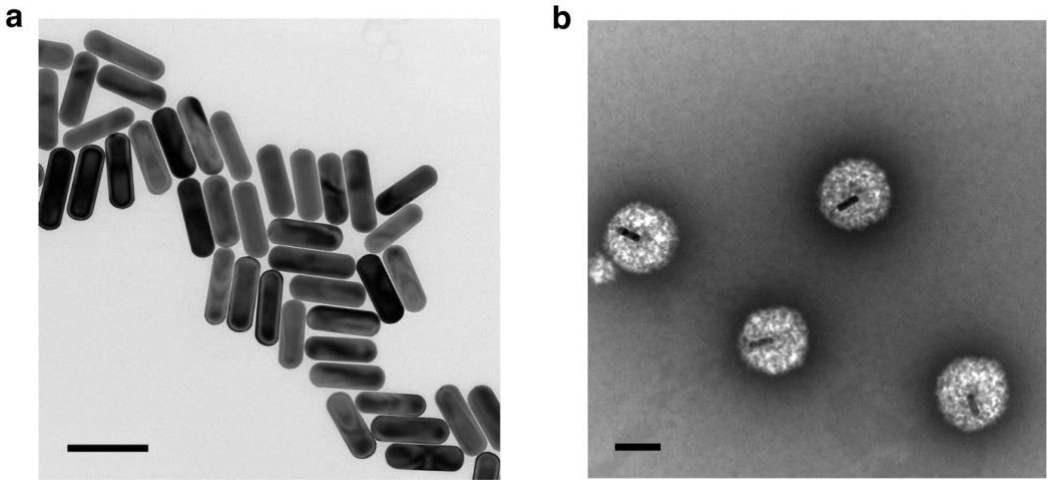

Fig. S1. Representative transmission electron microscopy (TEM) images of (a) the gold nanorods and (b) the nanoactuators. The scale bars show 100 nm.

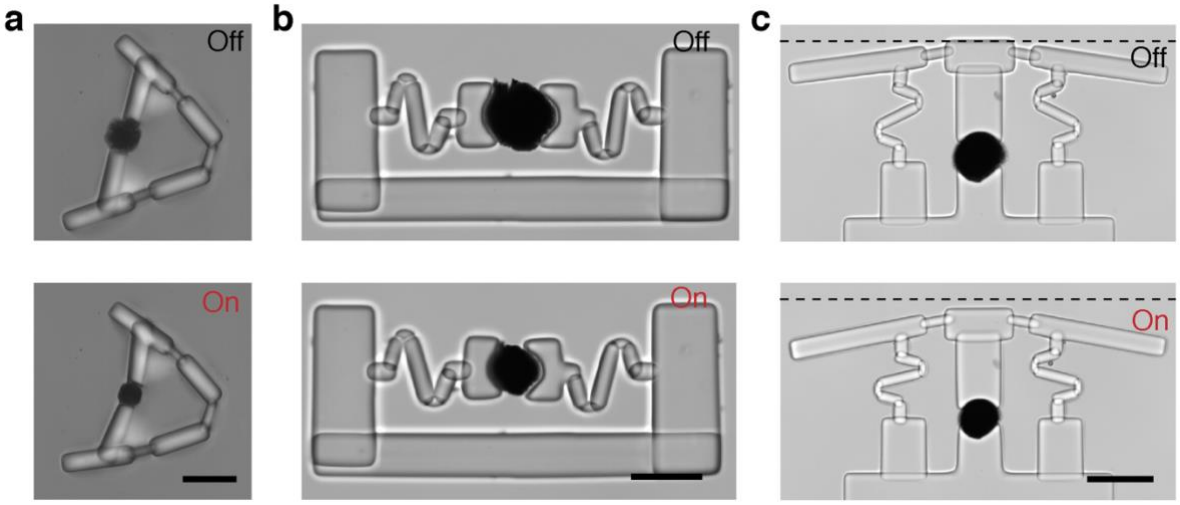

Fig. S2. Compliant mechanisms with multiple mechanical elements. (a) The actuation of a lever arm with multiple flexure hinges. The position of the hinges determines the overall deformation profile. (b) A serial double spring mechanism. The springs deform in response to actuator stress. (c) A parallel spring arrangement. This configuration aids the deformation along the pre-defined axis by eliminating out-of-axis movement. All scale bars, 100 µm.

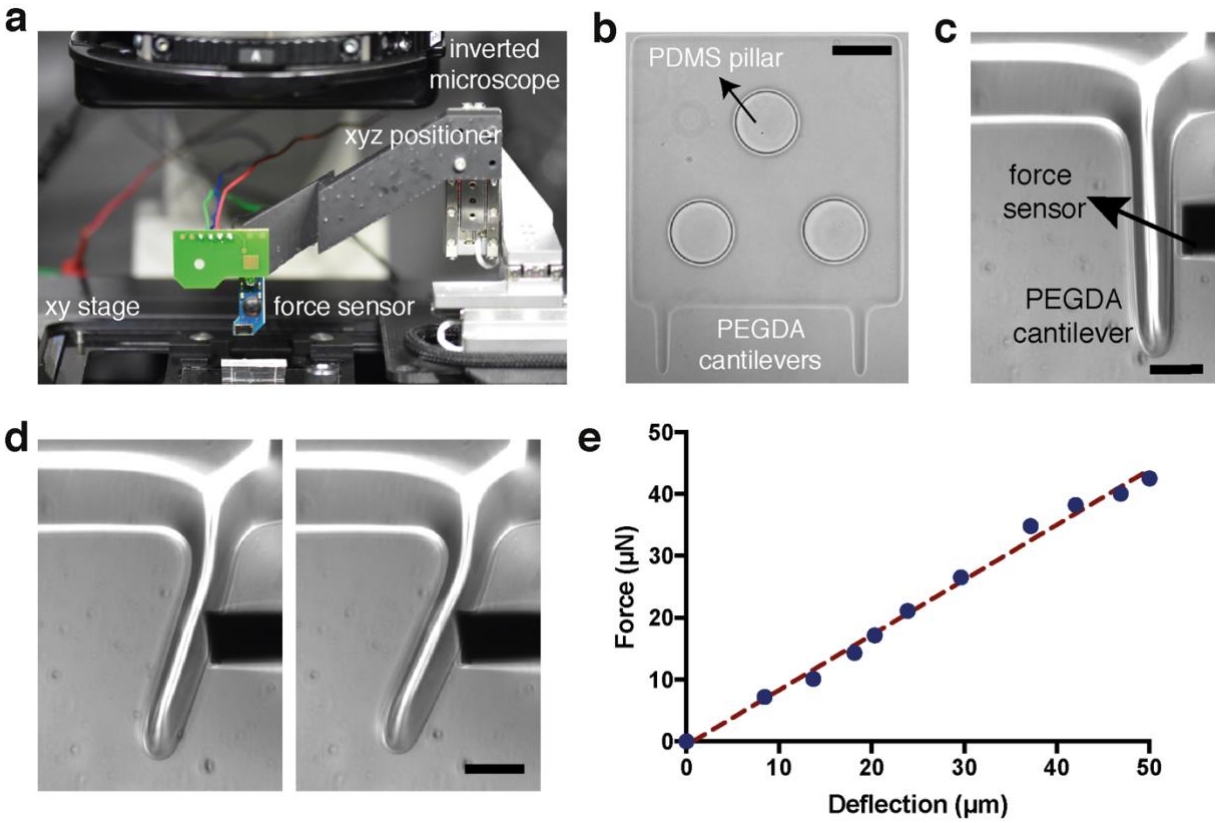

Fig. S3. Characterization of the bending modulus. **(a)** The position of the MEMS based capacitive force sensor is controlled by a motorized xyz micromanipulator while the position of the sample is controlled by the microscope stage. **(b)** The base of the cantilever device is polymerized directly around the PDMS micropillars using the digital maskless lithography system. The pillars stabilize the base and keep it stationary during bending tests. Scale bar, 100 μm. **(c)** Close-up of the cantilever beam and the tip of the sensor. Scale bar, 50 μm. **(d)** Snapshots from a representative microindentation experiment. Scale bar, 50 μm. **(e)** A representative force versus deflection curve. The slope of the linear fit is used for calculating the bending modulus.

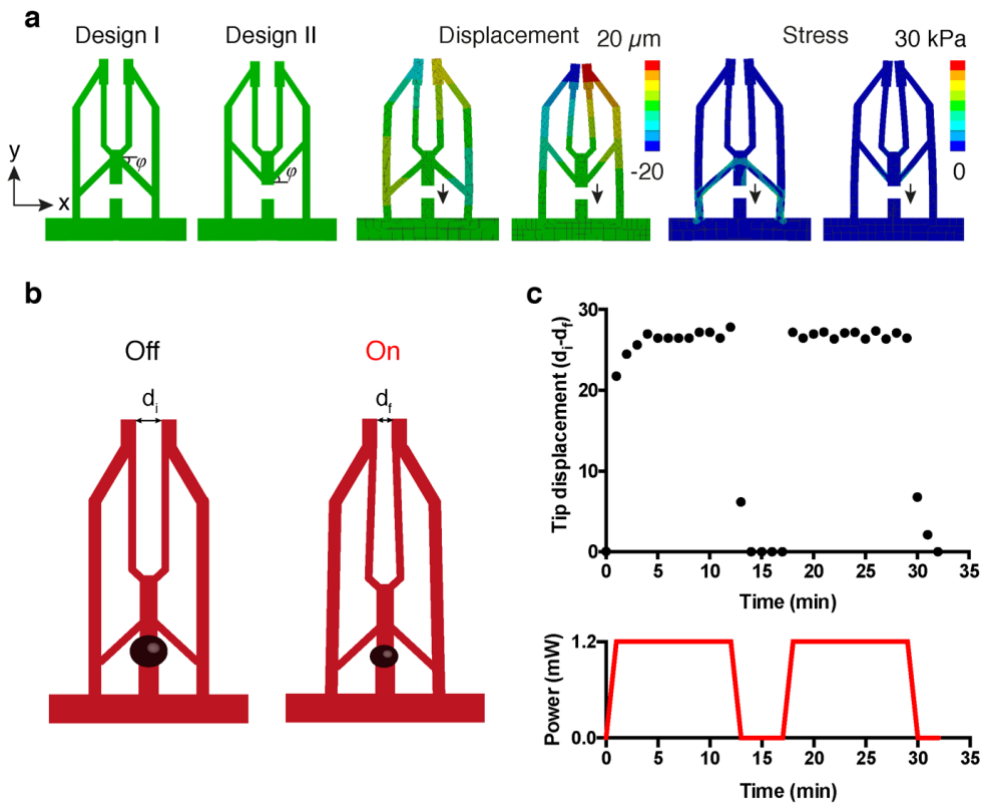

Fig. S4. (a) FEM simulations of two alternative gripper designs. Changes in the link angles result in significant variations in strain at the fingers and stress distribution in the skeleton. (**b)** Long-term activation of a microgripper device with the illustrated design. **(c)** The tip displacement of the gripper is plotted over time. The actuators can work robustly against the load for relatively long actuation periods. The results were replicated for six different microgrippers.

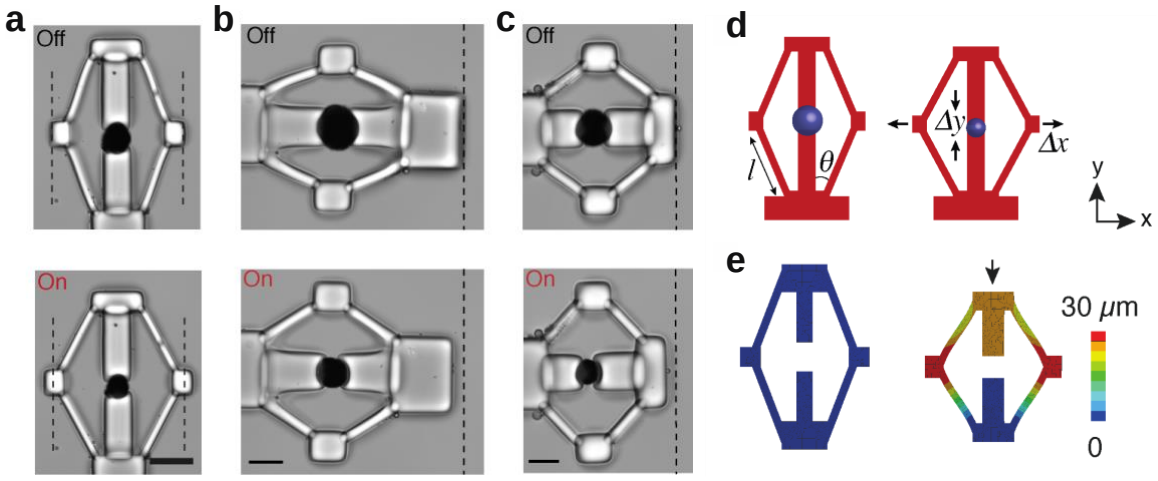

Fig. S5. (a-c) Flextensional mechanisms with different link angles (30° or 45°) and arm lengths (75 μm or 150 μm). All scale bars, 50 μm. **(d)** Schematic illustration of the flextensional mechanism denoting the input, output, and design parameters. **(e)** The FEM analysis of a representative example for a flextensional mechanism.

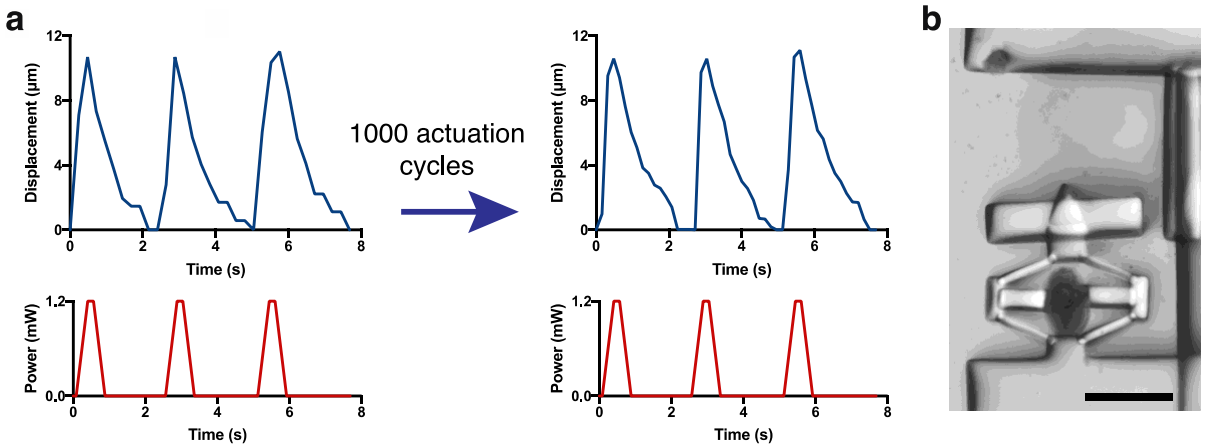

Fig. S6. Design and testing of the soft robotic compressor microdevice. (a) The displacement of the piston over time under repetitive laser stimulation. There was no detectable change in the performance of the device after 1000 actuation cycles. The laser power was set to 1.2 mW and the results were replicated for six different microdevices. (b) The design of the piston can be modified to tune the applied stress at a given strain. A representative example for a compression device with a sharp tip. Scale bar, 100 μm.

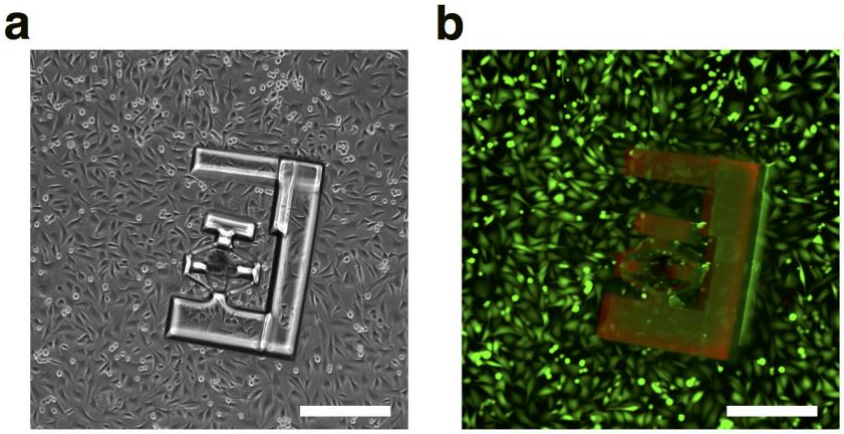

Fig. S7. Live/dead assay on the cell-seeded compression microdevice. Green color indicates live cells (calcein-AM) and red color indicates dead cells (ethidium homodimer-1). Scale bars, 200 μm.

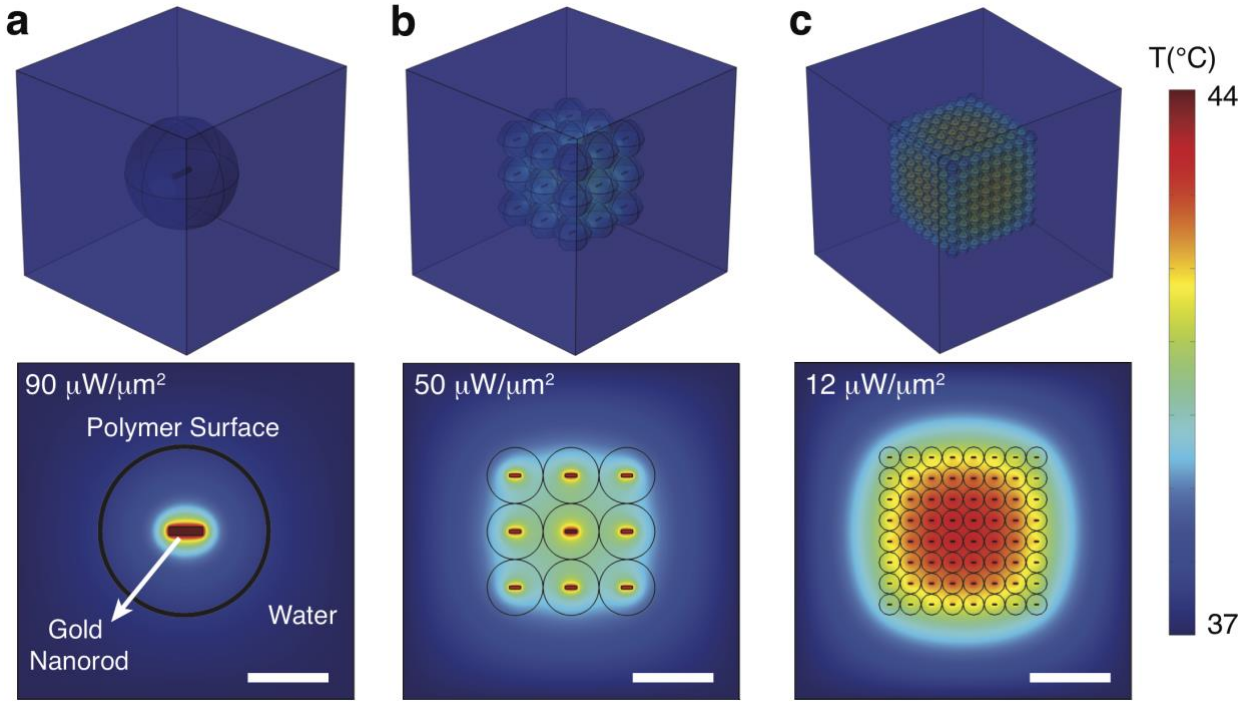

Figure S8 Finite element simulation of the heat distribution in NAs and MAs irradiated with NIR in water. Top, 3D view of a a) single NA, b) MA with 9 NAs packed together, and c) MA with 512 NAs arranged in packed together. Bottom, 2D cross-sectional view of the particles. The power required to reach LCST of the polymer depends on the number of particles in the agglomerate. The surface temperature stays slightly above the physiological ambient temperature while the core goes through thermally-induced contraction in all conditions. The scale bars are 250 nm, 750 nm, and 2 μm.

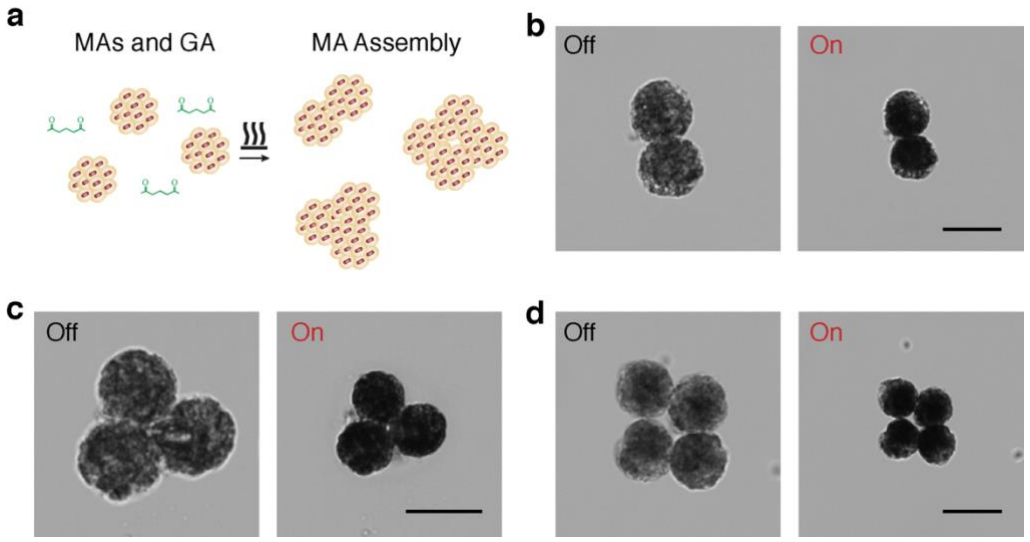

Fig. S9. Formation of multi-MA clusters. **(a)** A schematic representation of MA self-assembly inside microfabricated wells. **(b)-(d)** Optical images of dimers, trimers, and tetramers before and during NIR exposure. The assemblies stay intact after hundreds of actuation cycles. Scale bars, 50 μm.

Simulated body	Mesh size	Physics	Applied displacement	Young's modulus	Poisson's ratio
Flextensional mechanism	4 µm	Static structural	23.5 µm	500 kPa	0.33
Microgripper	3 µm	Static structural	7 µm	500 kPa	0.33
Continuum manipulator	2 µm	Static structural	10-15 µm	500 kPa	0.33

Table S1. Parameters used in the FEM analysis of solid deformation.

Video S1
Single twitch. The spherical MA deforms when actuated by the NIR laser and fully recovers its original shape when the laser is turned off. Movie is played in real-time.

Video S2
Frequency modulation of spherical MA actuation. The video shows the contraction and relaxation of a MA for different actuation frequencies, ranging from 2 to 4 Hz. Movie is played in real-time.

Video S3
Actuation of Type I and Type II lever systems. The position of the MA determines the angular displacement. Movie is played in real-time.

Video S4
Microgripper operation. The movie shows tweezers with direct connection on the left and with an additional flextensional mechanism on the right. The actuation of the MA generates closure of the fingers in the first prototype and opening of the fingers in the second prototype. Movie is played in real-time.

Video S5
Single twitch. The fiber MA deforms when actuated by the NIR laser and fully recovers its original shape when the laser is turned off. Movie is played in real-time.

Video S6
Frequency modulation of fiber MA actuation. The video shows the contraction and relaxation of a fiber MA for different actuation frequencies, ranging from 0.5 to 10 Hz. Movie is played in real-time.

Video S7
Microgripper actuated by an antagonistic fiber MA pair. Movie is played in real-time.